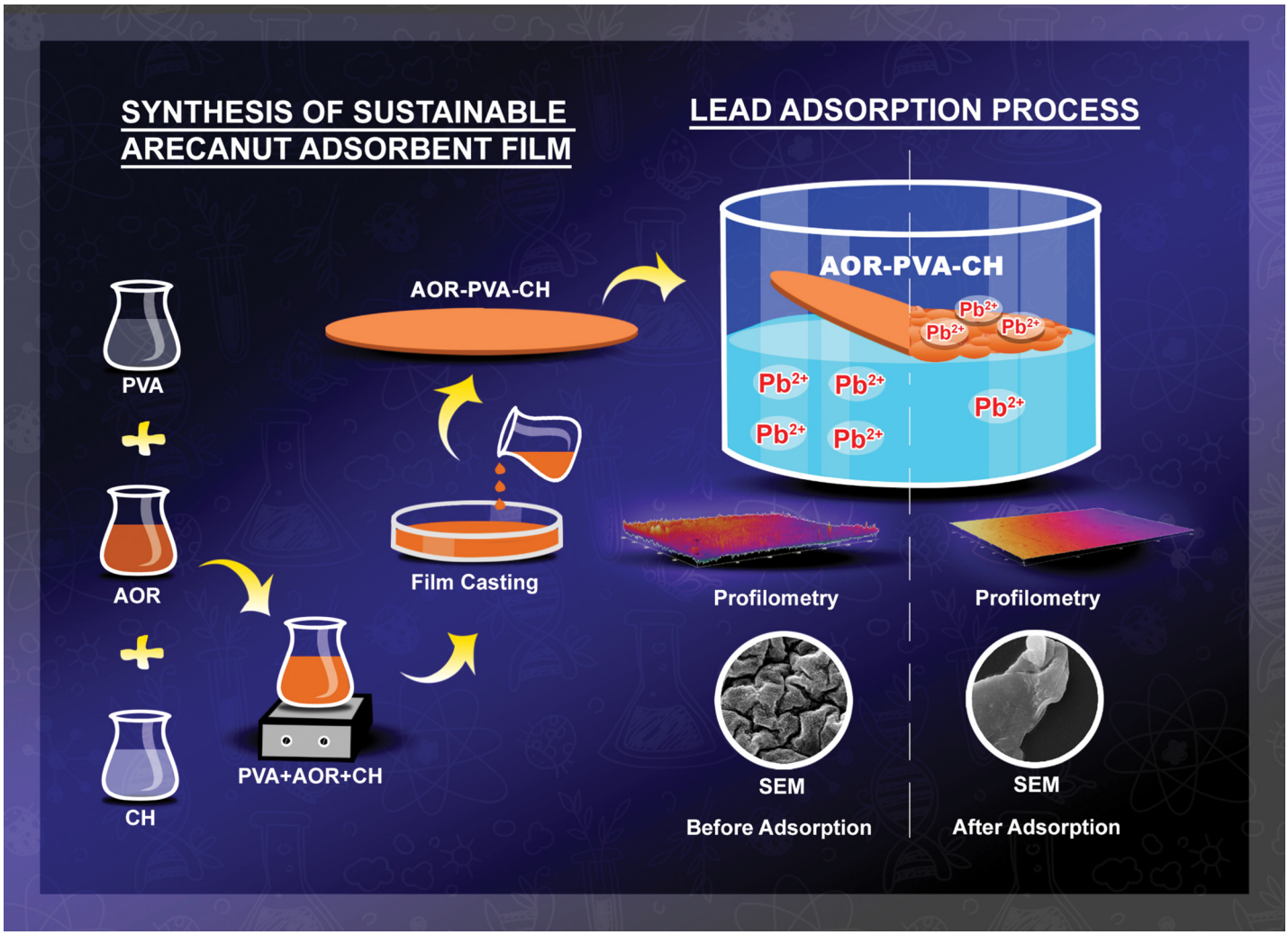

Showcasing research from Dr Vijayasankar AV's laboratory, Department of Chemistry, Christ University, Bangalore, India.

Sustainable fabrication of arecanut waste-based polymer blend adsorbents for enhanced lead(II) ion removal from water

This study presents a green and sustainable route for converting arecanut agricultural waste into efficient polymer blend adsorbent for Pb(II) removal from water. Incorporation of arecanut organic residue into a PVA–chitosan matrix enhances surface functionality and strengthens metal–ion interactions through hydroxyl and amine groups. The resulting films display improved adsorption capacity, favourable Langmuir isotherm behaviour, and rapid pseudo-second-order kinetics. Stable performance under optimized conditions highlights the potential of this low-cost, eco-friendly adsorbent for sustainable lead remediation in water systems.

Image reproduced by permission of Vijayasankar A.V. from *Mater. Adv.*, 2026, **7**, 1432.

As featured in:

See Vijayasankar A.V. *et al.*, *Mater. Adv.*, 2026, **7**, 1432.

ROYAL SOCIETY OF CHEMISTRY

rsc.li/materials-advances

Registered charity number: 207890

Materials Advances

ROYAL SOCIETY OF CHEMISTRY

PAPER

View Article Online
View Journal | View Issue

Cite this: *Mater. Adv.*, 2026, 7, 1432

Sustainable fabrication of arecanut waste-based polymer blend adsorbents for enhanced lead(II) ion removal from water

Jasmine Jose,[a] Binish CJ,[a] Jobish Johns,[b] Aniz CU,[c] Sony J. Chundattu[d] and Vijayasankar AV *[a]

Heavy metal contamination in water systems leads to critical environmental and health challenges, necessitating sustainable remediation technologies. This study presents a unique approach utilising arecanut organic residue, an abundant agricultural waste, for the removal of lead from water. A bio-adsorbent composite film was synthesised using chitosan–polyvinyl alcohol (PVA) incorporated with arecanut organic residue by solvent casting. The physicochemical properties of the films were characterised by XRD, FTIR, optical profilometry, BET surface area and SEM analyses. The adsorption efficiency of the synthesised films was tested by examining the removal of Pb(II) from water. The bioadsorbent films demonstrated a Pb(II) removal efficiency of 94.6% from 5 ppm solutions at pH 6 within 60 minutes at 70 °C using 0.5 g of the film. Optimisation studies revealed the critical role of functional group availability and film porosity of the polymer blends, along with experimental conditions that enhanced the adsorption capacity. Kinetic studies also confirmed the results obtained from the optimisation studies. The adsorption kinetics followed a pseudo-second-order model, and isotherm analysis confirmed Langmuir-type adsorption. The sustainable bioadsorbent exhibited good reusability, maintaining performance over multiple cycles.

Received 27th October 2025,
Accepted 30th December 2025

DOI: 10.1039/d5ma01239b

rsc.li/materials-advances

1. Introduction

The need for effective water treatment has become increasingly critical as industrial activity generates substantial amounts of organic and inorganic waste;[1] if left untreated, these wastes can lead to serious environmental and public health hazards. One of the most pressing environmental concerns is water pollution caused by toxic heavy metals, such as lead,[2] cadmium,[3] chromium[4] and mercury.[5] These contaminants primarily enter water sources through industrial activities, including mining,[6] smelting,[7] battery manufacturing,[8] and wastewater discharge.[9] Once released, heavy metals persist in the environment and bioaccumulate through food chains, posing severe risks to both human and ecological health.[10]

Among these pollutants, Pb(II) is of particular concern as it causes neurotoxicity, renal disorders, and developmental issues in children.[11] Its persistence in aquatic ecosystems and high toxicity highlight the urgent need for efficient and sustainable Pb(II) removal technologies to safeguard public health and environmental integrity.[12]

Traditional Pb(II) removal techniques, such as chemical precipitation,[13] ion exchange,[14] membrane filtration,[15] and electrochemical treatments,[16] have shown varying degrees of success. Yet, adsorption remains the most efficient, cost-effective, and simple method for removing lead ions from aqueous media.[17] As a result, recent research has focused on developing advanced adsorbent materials capable of selectively binding Pb(II) ions.[18,19] Table 1 presents a comparison of the lead removal efficiencies of various adsorbents reported in the literature. Various materials, including starch,[20] chitosan,[21] zeolites,[22] metal–organic frameworks,[23] magnetic materials,[24] carbon-based substances,[25] weathered coal,[26] and pottery granules,[27] have been applied as adsorbents for the removal of lead. Polymers and polymer blends have been reported as highly effective, biocompatible and nontoxic, cost-effective adsorbents for Pb(II) adsorption.[28,29] Polymer blends incorporating plant-based components, such as carboxycellulose nanofibers[30] and *Tacca leontopetaloides* biopolymer flocculants,[31] exhibit enhanced lead chelation while offering antioxidant benefits.

Polymers and polymer blends have notable advantages as adsorbents for lead removal from water; however, they also face

[a] *Department of Chemistry, Christ University, Bengaluru, 560029, India. E-mail: av.vijayasankar@christuniversity.in*
[b] *Department of Physics, Rajarajeswari College of Engineering, Mysore Road, Bengaluru, 560074, India*
[c] *Interdisciplinary Research Center for Refining and Advanced Chemicals (IRC-RAC), King Fahd University of Petroleum & Minerals, Dhahran, 31261, Saudi Arabia*
[d] *Department of Sciences and Humanities, Christ University, Bengaluru, 560074, India*

Table 1 Lead(II) removal efficiencies of bioadsorbents and polymer-based adsorbents reported in the literature

S. no	Adsorbent used	Experimental conditions	Maximum removal capacity for Pb(II) (%)	Ref.
1	Banana peels	Initial concentration 100 mg L^{-1}, pH 5, adsorbent dosage 1 g	88.94	38
2	Bagasse biochar	pH 5, contact time 140 min, adsorbent dosage 5 g, room temperature	75.376	39
3	Rice husk ash	pH 3.0	80	40
4	Mustard waste biomass	pH 5.5, 5.0 g biosorbent/L, contact time 2 hours, high temperature	94.56	41
5	Orange peel	Adsorbent dosage 1 g, initial concentration 10 mg L^{-1}	90	42
6	Cucumber peel	pH 5.0, initial Pb(II) concentration 25 mg L^{-1}, temperature 25 °C	93.5	43
7	*Azadirachta indica* leaves	Adsorbent dose 0.60 g, contact time 40 min, pH 7	93.5	44
8	PVA/α-manganese dioxide composite	Neutral to slightly acidic, room temperature	88.7	45
9	PVA/MWCNTs	pH 7, adsorbent dose 0.5 g, initial Pb(II) concentration 65 mg L^{-1}, contact time 300 min, room temperature	86	46
10	Chitosan/polyester crosslinking spheres	pH = 5.0	83.5	47

significant limitations related to their physical properties,[32] adsorption capacity, and post-use separation, which hinders their regeneration and operational efficiency.[33]

Many unmodified polymers also exhibit low adsorption capacity and selectivity, necessitating further chemical modification or blending; however, even these modifications of polymers often fail to maintain performance during repeated use. The effectiveness of polymer adsorbents is further limited by their sensitivity to process conditions, such as pH, temperature, and pollutant concentration and dosage, which reduces their reliability in water treatment applications.[34] Additional challenges include solubility and instability in aqueous media, which complicate separation and increase the risk of secondary contamination.[35] Complex synthesis procedures, high production costs, and limited scalability hinder large-scale implementation.

These challenges highlight the need for modification in the selection of raw materials, synthesis methods, physical stability, regeneration, and economic feasibility of advanced polymer-based bioadsorbents for large-scale sustainable water purification solutions.[36,37]

This study presents a bioadsorbent that effectively circumvents the limitations of traditional polymer and polymer blend-based adsorbents for Pb(II) removal in aqueous environments. A PVA–chitosan composite film incorporated with arecanut organic residue (AOR) was synthesised and deployed as an adsorbent for the removal of Pb(II) from water. The synthesised material exhibited enhanced adsorption capacity, coupled with stability and reusability. The sustainable and cost-effective raw materials extracted from agricultural waste, the facile synthesis protocol, and the potential for scalable manufacturing make the method and composite film a highly promising, environmentally friendly solution for lead removal. The present investigation is unique due to the development of a highly efficient adsorbent that outperforms several reported materials in Pb(II) removal, emphasizing its practical significance for advanced wastewater treatment.

2. Materials and methods

PVA of analytical grade with a molecular weight of 22 000 was sourced from Merck. The medium molecular weight chitosan (190 000–310 000 Da), which has a 75% to 85% deacetylation degree, was acquired from Merck, India. The organic residue extracted from arecanut (AOR) was collected from an arecanut factory located in Mangalore, India. Lead nitrate with 99% purity was obtained from Merck, India. The chemicals used for colorimetric studies, 1,5-diphenylthiocarbazone (dithizone, analytical grade), 2-propanol (HPLC grade), hydrochloric acid (37%, reagent grade), and cetyltrimethylammonium bromide (CTAB, analytical grade), were obtained from Merck.

The physicochemical properties of the synthesised AOR–PVA–CH blends were examined by various methods. BET surface area measurements were performed using Quantachrome Instruments (version 1.24). X-ray diffraction analysis was performed on a Rigaku Miniflex 600 X-ray diffractometer. FTIR analysis was carried out with a Bruker Alpha II FTIR spectrometer. Optical profilometry of the blends was performed using a Zeta 20 optical profilometer (KLA Tencor). Scanning electron microscopy images were captured using an Apreo 2S instrument. The concentration of Pb(II) adsorbed was determined using a Vernier Pro colorimeter.

2.1. Synthesis of AOR–PVA–CH blends

A homogeneous solution of organic residue from arecanut (AOR) was extracted by boiling mature arecanuts in distilled water for 30 minutes. The boiled mixture was filtered, and the dense residual liquid was collected as the arecanut organic extract. 1 g of polyvinyl alcohol (PVA) was added to 50 mL of water, and the mixture was stirred at 80 °C using a magnetic stirrer for 15 minutes until fully dissolved. A series of chitosan solutions in acetic acid was prepared by varying the amount of chitosan from 0.3 to 0.4 g. Chitosan was dissolved in a 1% acetic acid–water mixture (50 mL) and stirred at 80 °C for 15 minutes until a smooth, uniform solution was formed. After mixing the homogeneous PVA solution with 1 mL of AOR solution, the chitosan solution was added. The resulting blend was stirred continuously at 60 °C using a magnetic stirrer and sonicated for 3 hours to ensure complete homogeneity. The final blend was cast into films using the solution casting technique and then dried for 1.5 days at 60 °C in a hot air oven. The uniformity in thickness was ensured by pouring 45 mL of solution into the Petri dish, which was found to be 0.2 mm. The BET surface area and porosity of the synthesised samples were analysed and given in Table 2. The surface

Table 2 Composition and porous properties of pure PVA, pure chitosan and AOR–PVA–CH blends

Film	Amount of chitosan (g)	BET surface area ($m^2\ g^{-1}$)	BJH pore volume (cc g^{-1})	BJH pore radius (nm)
AOR-C1	0.3	38	0.0430989	1.68349
AOR-C2	0.325	42	0.0252634	1.8902
AOR-C3	0.35	57	0.0180516	1.68374
AOR-C4	0.375	44	0.0133212	1.88242
AOR-C5	0.4	39	0.0138049	2.40121
PVA	—	30.61		
CH	0.35	29.84		

The amount of AOR and PVA was kept constant.

area of the samples increases with the increase in the amount of chitosan until 0.35 g, which is considered the optimum amount. Further increase in the amount of chitosan in the blend leads to a decrease in surface area and pore volume.

2.2. Adsorption studies

The adsorption efficiency of the synthesised polymer blend films was tested by submerging 0.1 g of film for 30 minutes in 10 ml of 1 ppm Pb(II) solution. The concentration of Pb(II) was determined using 1,5-diphenylthiocarbazone (dithizone) and cetyltrimethylammonium bromide (CTAB), which acts as a surfactant. The submerged film was tested for the concentration of Pb(II) adsorbed by the film using a Vernier Pro colorimeter, operating at 520 nm.

A 1 ppm Pb(II) standard solution was combined with 1.5 mL of 0.000195 M dithizone solution, 1.0 mL of 0.004 M HCl, and 4.0 mL of 0.3 M CTAB, followed by the addition of 1.0 mL of the sample solution in a 10 mL calibrated volumetric flask. The resulting mixture was diluted to the mark with deionised water, thoroughly homogenised, and allowed to stand for equilibration prior to measurement.

The AOR–PVA–CH blend films, prepared with varying weight ratios, were used as adsorbents to remove Pb(II) and the removal efficiency of Pb(II) ions was calculated using the following equation:[48]

$$\text{Removal efficiency} = \frac{(C_i - C_e)}{C_i} \times 100$$

where C_i represents the initial concentration of Pb(II) and C_e denotes the equilibrium concentration.

The removal efficiency of the AOR–PVA–CH blends at various molar ratios is given in Table 3. Among the tested samples, the AOR-C3 film demonstrated the highest removal efficiency for Pb(II). Consequently, the AOR-C3 film was deployed as an adsorbent for further optimisation studies, including adsorbent dosage, contact time, initial concentration, pH and temperature during adsorption. All experiments were repeated to ensure reproducibility and statistical reliability of the results.

Table 3 Removal efficiency of the pure PVA, pure chitosan and AOR–PVA–CH blends

Film	Removal efficiency of film (%)
AOR-C1	42.12
AOR-C2	46.54
AOR-C3	52.4
AOR-C4	44.52
AOR-C5	40.21
PVA	32.26
CH	26.24

The amount of film used is 0.1 g, duration – 30 minutes, concentration of Pb(II) solution – 1 ppm.

3. Results and discussion

3.1. X-ray diffraction analysis

X-ray diffraction (XRD) analysis was performed to investigate the structural properties of the synthesised polymer blend films, as illustrated in Fig. 1. Pure chitosan exhibited two strong characteristic peaks at 2θ = 11° (110 plane) and 20.48° (020 plane). The peak at 11° is attributed to the acetylated amine group (N–CO–CH_3) in chitosan and denotes the intermolecular spacing between polymer chains,[49] and the peak at 20.48° is attributed to the free amine group (NH_2).[50]

Pure PVA displayed two distinct peaks at 2θ = 19.2°, corresponding to the (101) crystalline plane,[51] and 41.2°, corresponding to the 220 plane.[52]

In the polymer blend films, the characteristic peaks are observed at 2θ = 19.6°, when the peak at 2θ = 11° disappeared, which is attributed to hydrogen bonding interactions of the

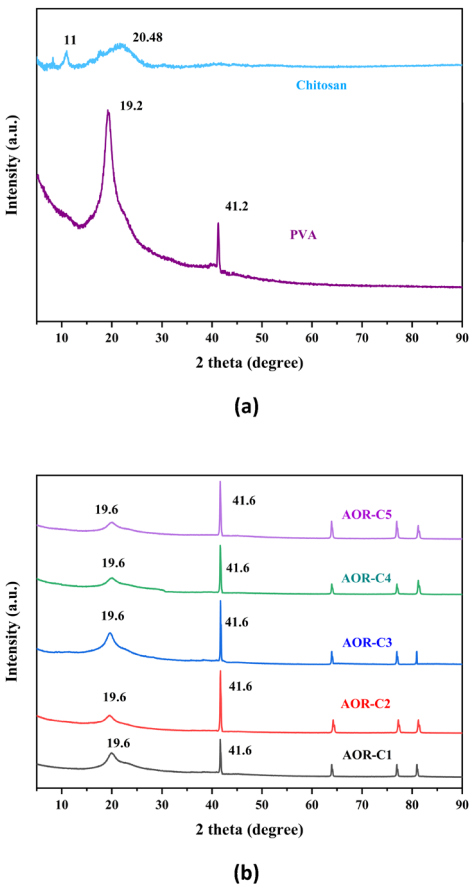

Fig. 1 (a) XRD patterns of pure PVA and pure chitosan. (b) XRD patterns of the AOR–PVA–CH blends.

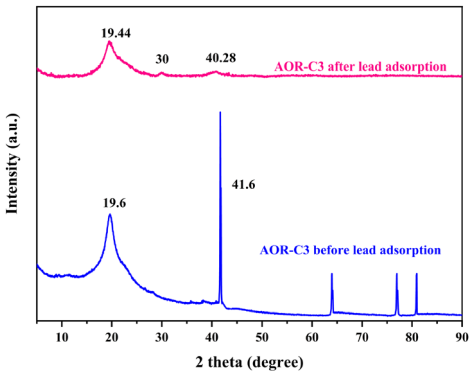

Fig. 2 XRD patterns of the AOR-C3 film before and after adsorption.

amine groups of chitosan and AOR with the hydroxyl groups of PVA.[53]

The XRD patterns of AOR-C3 before and after lead adsorption, as depicted in Fig. 2, illustrate significant structural changes in the material. A new peak observed around $2\theta = 30^{\circ}$ is attributed to the formation of lead compounds such as lead hydroxide, confirming the successful adsorption of lead ions.[54,55] The peak at $2\theta = 19.6^{\circ}$ shifts to $2\theta = 19.44^{\circ}$ with increased intensity. The peak shifts and peak broadening highlight the adsorption of lead ions over the surface of the polymer blend.

3.2. FTIR studies

The FTIR spectra of pure polyvinyl alcohol (PVA), pure chitosan and AOR–PVA–CH composite blends reveal characteristic functional group vibrations, providing insights into the interactions and composition of the materials, as shown in Fig. 3. The pure PVA spectrum shows a prominent hydroxyl (OH) stretching vibration at 3275 cm^{-1} due to intra-molecular hydrogen bonding between polymer chains.[56] The 2928 cm^{-1} band corresponds to the C–H stretching vibration of the alkyl groups in the polymer backbone, while the 1419 cm^{-1} and 1327 cm^{-1} bands are associated with C–H bending.[57] The C–O stretching vibration of the alcohol group is observed at 1093 cm^{-1}, further confirming the structure of the polymer.[58] The band observed at 916 cm^{-1} corresponds to CH_2 rocking vibrations,[59] while the band at 832 cm^{-1} is attributed to C–C stretching of PVA.[57,60]

In the case of pure chitosan, the broad band between 3200 and 3300 cm^{-1} is attributed to the combined OH and NH stretching, which is indicative of the amine and hydroxyl groups present in the structure.[61] The 1646 cm^{-1} band represents the amide C=O stretching vibration, while the 1545 cm^{-1} band corresponds to the N–H bending, further confirming the amide functionality in chitosan.[62] The C–O stretching vibrations are visible at 1063 cm^{-1} and 1022 cm^{-1}, and the band at 891 cm^{-1} is attributed to the C–H bending of the monosaccharide ring in the chitosan structure.[61,62]

The FTIR spectrum of the synthesised AOR–PVA–CH blend shows characteristic bands corresponding to the functional groups of its components, confirming successful blending. A broad band at 3290 cm^{-1} corresponds to –OH and –NH stretching vibrations, with a shoulder at 3660 cm^{-1} due to the new hydrogen bonding between the hydroxyl groups and amino

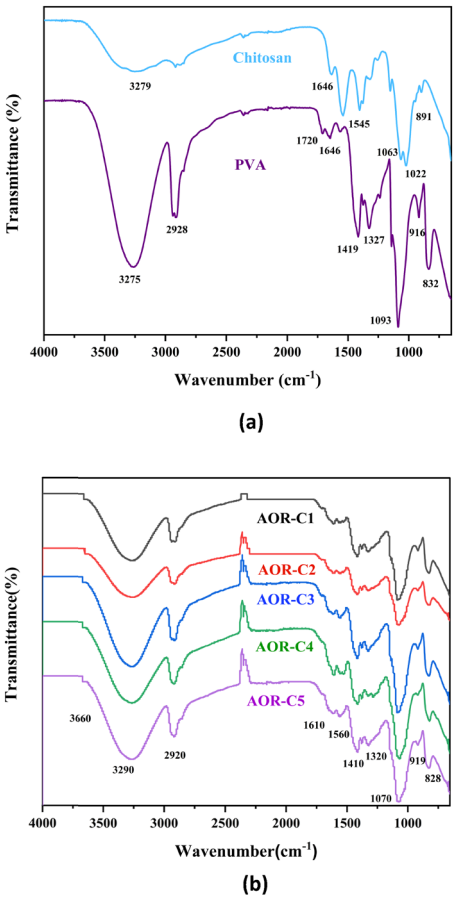

Fig. 3 (a) ATR-FTIR spectra of pure PVA and pure chitosan. (b) ATR-FTIR spectra of AOR–PVA–CH blends.

groups of PVA, chitosan and arecanut. The shifts in intensities and position of the FTIR peaks of the individual pure components indicate the formation of a homogeneous blend without chemical modification of the individual components.[63]

The FTIR analysis of the AOR-C3 before and after lead adsorption is depicted in Fig. 4. A new shoulder peak appears at 2849 cm^{-1} after adsorption, which may correspond to CH_2 stretching vibrations affected by lead ion binding.[64] The C–O stretching band at 1070 cm^{-1} shifts to 1041 cm^{-1}, and the –NH bending band at 1560 cm^{-1} shifts to 1558 cm^{-1} due to coordination of Pb^{+2} to oxygen and nitrogen sites.[65] The band at 919 cm^{-1} disappears after adsorption, indicating that the CH_2 rocking vibration is altered or suppressed upon interaction with lead. The observed changes in the FTIR bands indicate that lead adsorption primarily involves interactions with the hydroxyl, amine, and carboxyl groups in the AOR-C3 structure.

3.3. Optical profilometry

In our study, we analysed the surface roughness of five different samples using key roughness parameters, namely average roughness (R_a), maximum peak height (R_p), maximum valley depth (R_v), and kurtosis (R_{ku}), as tabulated in Table 4. AOR-C1 exhibited high R_p (60.65 nm) and R_v (75.63 nm) values, indicating the presence of non-uniform peaks and valleys on its

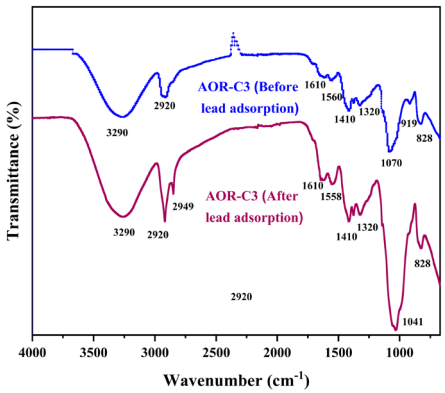

Fig. 4 ATR-FTIR spectra of the AOR-C3 film before and after adsorption.

Table 4 Result of optical profilometry of the synthesised AOR–PVA–CH blends and AOR-C3 after lead adsorption

Samples	R_a value	R_p value	R_v value	R_{ku} value
AOR-C1	11.05	60.65	75.63	3.660
AOR-C2	6.806	74.78	28.44	8.807
AOR-C3	15.92	320.90	148.59	25.93
AOR-C4	10.28	71.32	99.32	4.053
AOR-C5	7.000	66.35	61.25	5.454
AOR-C3 (after lead adsorption)	1.498	14.39	27.73	23.28

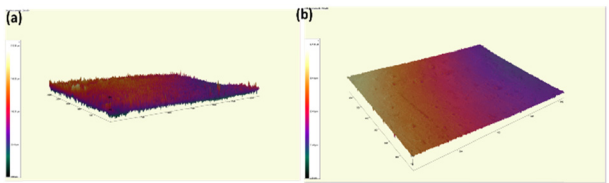

Fig. 5 Surface roughness of the AOR-C3 film (a) before lead adsorption and (b) after lead adsorption.

surface. AOR-C3, with the highest R_a (15.92 nm), R_p (320.9 nm), R_v (148.59 nm), and an exceptionally high R_{ku} (25.93), showed significant surface irregularities and sharp features, suggesting a highly textured and rough surface, as evident from Fig. 5. Comparatively, AOR-C2, AOR-C4, and AOR-C5 exhibited more moderate surface roughness parameters, indicating smoother and more uniform surfaces. This suggests that AOR-C3, with its rougher and more varied surface, may possess superior adsorption properties,[66] making it more effective for applications requiring high surface interaction.

After adsorption, the synthesised films exhibited a significant reduction in surface roughness, which indicates the adsorption of Pb(II) over the surface of the adsorbent. This reduction was further validated by the disappearance of specific peaks in the XRD patterns and FTIR spectra before and after adsorption.

3.4. SEM

Scanning electron microscopy (SEM) was employed to investigate the surface morphology and structural features of the

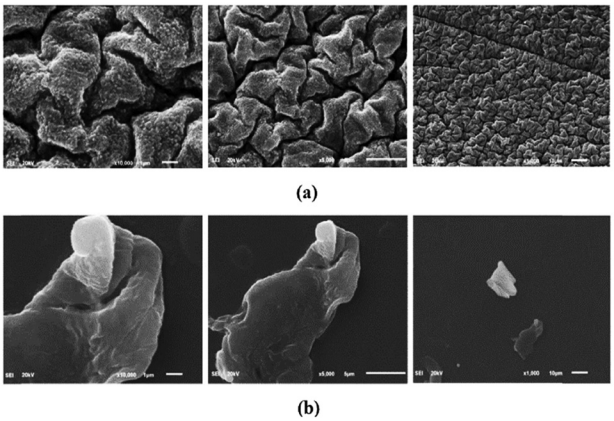

Fig. 6 SEM images of the AOR-C3 film (a) before lead adsorption and (b) after lead adsorption, captured at different magnifications: 1 μm, 5 μm and 10 μm.

blends. As shown in Fig. 6, the film surface before adsorption displays a relatively uniform and interconnected morphology, indicating good dispersion of the arecanut organic residue (AOR) within the polymer matrix and strong compatibility between the blend components. SEM images before and after lead adsorption, with different magnifications, reveal distinct morphological structures. After Pb(II) adsorption, the SEM images reveal a mixture of dark and bright regions across the film surface, along with a smoother morphology, confirming the successful adsorption of Pb(II) onto the film surface.[45]

3.5. Optimisation studies

The optimisation experiments were conducted using 10 mL of Pb(II) solution under varying conditions to understand their effect on adsorption. The parameters studied included adsorbent dosage (0.1–0.7 g), contact time (15–90 minutes), initial Pb(II) concentration (0.5–30 ppm), pH of the Pb(II) solution (2–9) and temperature (30–90 °C).

3.5.1. Effect of adsorbent dosage. The adsorbent dosage was varied from 0.1 to 0.7 g to assess its impact on Pb(II) removal. The experiments were conducted at 40 °C for 30 minutes with an initial Pb(II) concentration of 1 ppm. As illustrated in Fig. 7, the removal efficiency increased with adsorbent dosage due to the

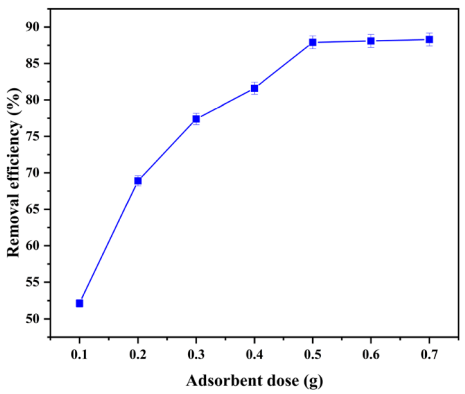

Fig. 7 Effect of adsorbent dose on Pb(II) removal by the AOR-C3 film.

greater availability of surface area and active sites.[67] Furthermore, the increased surface area reduces diffusional resistance and shortens the path length that lead ions must traverse to reach unoccupied sites, thereby accelerating the adsorption kinetics. The optimal dosage was determined to be 0.5 g, at which the maximum removal efficiency was achieved. Once all Pb(II) ions have been adsorbed, the addition of excess adsorbent merely increases the proportion of unutilized active sites without contributing to enhanced removal. This results in a decrease in adsorption capacity with increasing dosage beyond the optimum, even though the percentage removal may remain constant. The reduction occurs because the same amount of adsorbate is distributed among a greater mass of adsorbent, leading to underutilization of the available binding sites. The optimal adsorbent dosage of 0.5 g for the AOR-C3 film in Pb(II) removal from 1 ppm solutions represents the critical point where the maximum removal efficiency is achieved through complete utilisation of the available adsorbate while maintaining effective dispersion of the active sites. Beyond this dosage, no significant improvement was observed, as the adsorption sites became saturated. Thus, 0.5 g of AOR-C3 film was considered the ideal dosage for further studies.

3.5.2. Effect of contact time. The effect of contact time on Pb(II) adsorption was evaluated by varying the time from 15 to 90 minutes at 40 °C. Using 0.5 g of AOR-C3 film and 1 ppm Pb(II) solution, the adsorption rate was initially rapid due to the abundant availability of active sites.

As adsorption progressed, the high-affinity sites were gradually occupied, leaving behind sterically hindered or lower-energy sites that were less favourable for binding. Electrostatic repulsion between the adsorbed Pb(II) ions on the film surface and those remaining in solution further reduced the adsorption rate,[68] and the equilibrium was reached after approximately 60 minutes, as shown in Fig. 8, representing the dynamic state where the rate of adsorption equals the rate of desorption. At this point, no net change in Pb(II) concentration occurs in either the solution or on the adsorbent surface.

Film diffusion dominates during the initial rapid adsorption phase, while intraparticle diffusion becomes increasingly important as external sites become saturated. The results observed on contact time-dependent behaviour suggest that the adsorption process follows pseudo-second-order kinetics, which is characteristic of chemisorption mechanisms involving valence forces through electron sharing or transfer between Pb(II) ions and the functional groups on the adsorbent surface. This kinetic model assumes that the rate-limiting step involves chemical interaction between the metal ions and the adsorbent, rather than simple physical adsorption.

A contact time of 60 minutes was found to be optimal for further studies. The relatively short equilibrium time (60 minutes) compared to that of many conventional adsorbents[69] demonstrates the high efficiency of the PVA–chitosan–AOR composite film and suggests favourable mass transfer characteristics suitable for lead removal applications.

3.5.3. Effect of initial Pb(II) ion concentration. The effect of initial Pb(II) concentration on adsorption was investigated by varying the concentration from 0.5 ppm to 30 ppm. Under optimal conditions of 0.5 g of AOR-C3 film, 60 minutes contact time, and 40 °C, the results (Fig. 9) indicated that the removal efficiency was highest at lower concentrations, which can be attributed to a favourable surface area-to-ion ratio, meaning that more active sites were available per Pb(II) ion. At higher concentrations, the active sites on the adsorbent become saturated,[70] forcing excess Pb(II) ions to compete for the remaining lower-affinity or sterically hindered sites, which leads to a decline in removal efficiency. The removal efficiency is highest at low concentrations and decreases as concentration increases, which is consistent with a Langmuir-type adsorption mechanism involving monolayer coverage of a finite number of homogeneous or heterogeneous binding sites.

The favourable adsorption at low concentrations, as reflected by the high removal efficiency at 5 ppm, suggests that the adsorbent–adsorbate interaction is thermodynamically favourable and that the binding process is largely irreversible under the experimental conditions. Maximum removal efficiency (92.38%) was observed at an initial concentration of 5 ppm, making it the ideal concentration for further investigations. This concentration-dependent behaviour provides valuable mechanistic insights and establishes 5 ppm as the ideal concentration for subsequent investigations aimed at further characterising the adsorption kinetics, thermodynamics, and

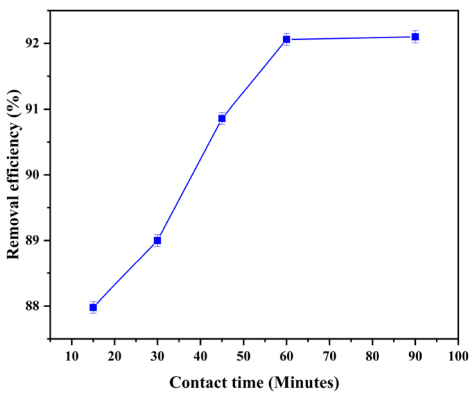

Fig. 8 Effect of contact time on Pb(II) removal by the AOR-C3 film.

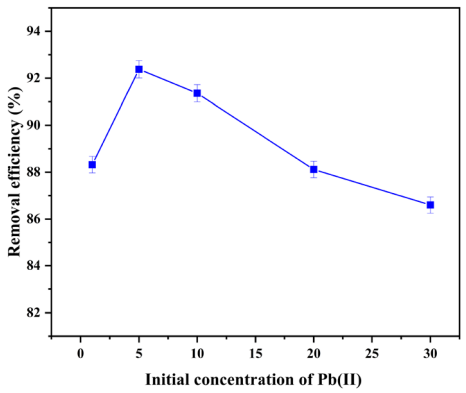

Fig. 9 Effect of initial concentration of Pb(II) of the AOR-C3 film on Pb(II) removal.

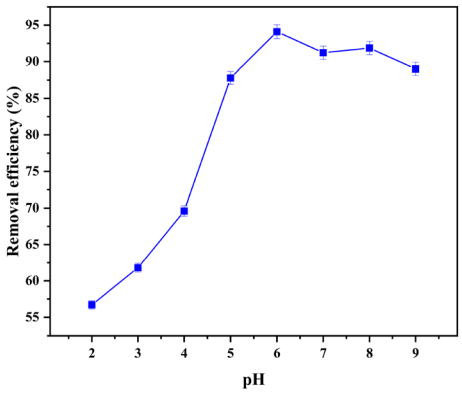

Fig. 10 Effect of pH on Pb(II) removal by the AOR-C3 film.

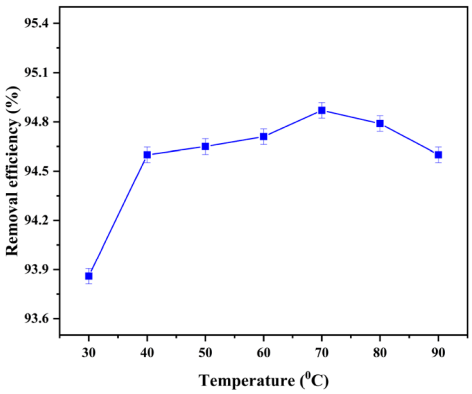

Fig. 11 Effect of temperature on Pb(II) removal by the AOR-C3 film.

regeneration potential of the AOR-C3 film adsorbent for lead ion removal applications.

3.5.4. Effect of pH. The effect of pH on Pb(II) adsorption was assessed by adjusting the pH from 2 to 9, maintaining 0.5 g of AOR-C3 film, a 5 ppm Pb(II) solution, and 60 minutes of contact time at 40 °C. The results given in Fig. 10 showed a significant pH-dependent behaviour of the AOR-C3 film with maximum removal efficiency at pH 6, reduced efficiency at acidic pH values, a slight increase at pH 8, and a subsequent decline beyond pH 8.

The highest removal efficiency was obtained at pH 6. At lower pH values, excess hydrogen ions competed with Pb(II) ions for adsorption sites, reducing efficiency.[71] Under acidic conditions, a high concentration of protons can easily protonate the functional groups on the adsorbent, particularly hydroxyl (–OH), and amino ($-NH_2$) groups. This extensive protonation results in a positive surface charge on the adsorbent film, creating strong electrostatic repulsion between the positively charged surface and the Pb(II) cations in solution. Beyond electrostatic repulsion, hydrogen ions physically occupy the binding sites that would otherwise be available for Pb(II) coordination.

At pH 8 there is a slight increase from the neutral pH as there is an electrostatic attraction for positive lead ions and there is less chance for lead hydroxide formation. Beyond pH 8, the formation of lead hydroxide precipitates caused a decline in removal efficiency. pH adjustments were made using phosphate buffer solution, and the pH was monitored using a pH meter.

3.5.5. Effect of temperature. According to our previous TGA studies,[60] arecanut organic residue–based films exhibit enhanced thermal stability, as evidenced by a delayed onset of degradation and higher decomposition temperatures compared to pure PVA and PVA–CH films. This improvement indicates increased resistance to thermal decomposition, attributed to strong interfacial interactions within the polymer matrix. The role of temperature in Pb(II) adsorption was investigated by adjusting the temperature from 30 °C to 90 °C, while maintaining optimal conditions of 0.5 g of the AOR-C3 film, pH 6, and 5 ppm Pb(II) solution for 60 minutes. As shown in Fig. 11, the removal efficiency increased with temperature up to 70 °C, attributed to enhanced molecular motion and interaction at higher temperatures. At elevated temperatures, the formation of coordinate bonds between Pb(II) ions and the electron-donating groups (nitrogen and oxygen atoms) on the polymer blend becomes more favourable. The positive enthalpy change ($\Delta H^\circ > 0$) calculated from thermodynamic analysis confirms the endothermic nature of the adsorption process in this temperature range.[72–74] However, at temperatures above 70 °C, a significant decline in adsorption efficiency was observed, which can be attributed to the increase in thermal energy becoming sufficient to overcome the binding energy between Pb(II) ions and the adsorbent surface, which leads to the desorption of previously adsorbed Pb(II) ions back into the solution, where the desorption rate will be more than the adsorption rate.

Based on these results, 70 °C was identified as the optimal temperature for the Pb(II) adsorption process using PVA–chitosan–arecanut extract composite films. The temperature-dependent behaviour demonstrates the correlation of endothermic adsorption and exothermic desorption processes, emphasizing the critical importance of temperature optimisation for effective lead removal from water.

3.6. Kinetic studies

Kinetic studies of lead adsorption onto the AOR–PVA–CH blend provide critical insights into the mechanism and efficiency of the adsorption process. The kinetic data were investigated using various models, including pseudo-first-order and pseudo-second-order, and are given in Fig. 12, to determine the rate-limiting step and the adsorption capacity of the film. Fig. 12a presents the pseudo-first-order kinetic plot, which exhibits a weaker linear correlation (R^2 = 0.8955), suggesting that the pseudo-first-order model does not adequately describe the adsorption kinetics of Pb(II) onto the film. All of the kinetic parameter values are listed in Table 5. According to the findings, the adsorption process adhered to a pseudo-second-order kinetic model (R^2 = 0.9987). Chemisorption is suggested as the dominant mechanism in the adsorption of Pb(II) onto the film, where the metal ions form strong chemical bonds with active sites on the surface of the material. The rate-determining step in this adsorption process is influenced by the film

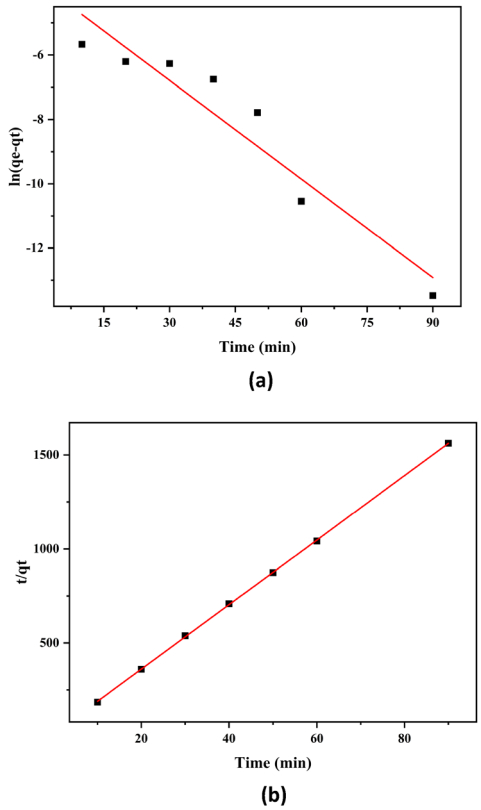

Fig. 12 (a) Pseudo-first-order kinetics for Pb(II) adsorption onto AOR–PVA–CH composite blends and (b) pseudo-second-order kinetics for Pb(II) adsorption onto AOR–PVA–CH composite blends.

Table 5 Kinetic parameters for the pseudo-first-order and pseudo-second-order reactions

Order of the reaction	Kinetic parameters and values
Pseudo-first-order	k_1 (min^{-1}) = 0.1020 q_e (mg g^{-1}) = 0.02429 R^2 = 0.8955
Pseudo-second-order	k_2 (g mg^{-1} min^{-1}) = 26.64 q_e (mg g^{-1}) = 0.003350 R^2 = 0.9987

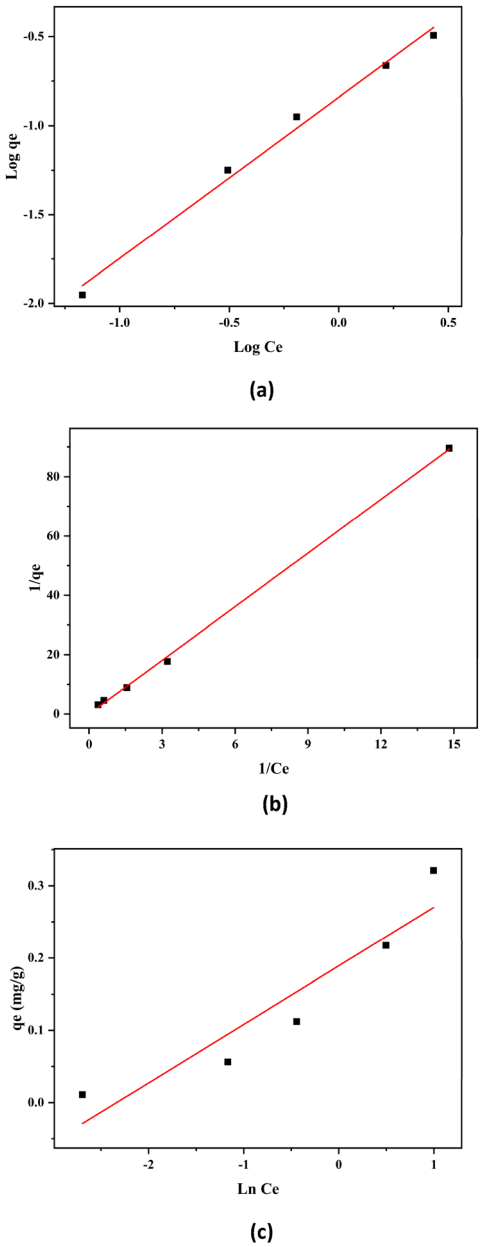

Fig. 13 (a) The Freundlich isotherm illustrating the adsorption of Pb(II) onto AOR–PVA–CH composite blends, (b) the Langmuir isotherm illustrating the adsorption of Pb(II) onto AOR–PVA–CH composite blends, and (c) the Temkin isotherm illustrating the adsorption of Pb(II) onto AOR–PVA–CH composite blends.

concentration, which determines the available active sites, and the concentration of Pb(II), which governs the driving force for the interaction of metal ions and the adsorbent surface. The results of the effect of contact time also confirmed that the adsorption process follows pseudo-second-order kinetics and chemisorption mechanisms, rather than physical adsorption, due to the functional groups on the adsorbent surface.

To elucidate the surface characteristics and the binding mechanism of the AOR–PVA–CH blend, three adsorption isotherm models – Freundlich, Langmuir and Temkin – were evaluated and are shown in Fig. 13. Values of all the parameters are included in Table 6. Among these, the Langmuir model demonstrated the highest correlation with the experimental data (R^2 = 0.9988), surpassing the Freundlich (R^2 = 0.9882) and Temkin (R^2 = 0.8405) models. This proves that the adsorbent exhibits monolayer adsorption with a homogeneous surface, where all active sites are identical and energetically equivalent. The optimisation results for the initial lead concentration given in Fig. 9 further confirmed the Langmuir-type adsorption mechanism, as the removal efficiency was highest at lower lead concentrations and gradually decreased with increasing concentration.

3.7. Reusability and regeneration of the adsorbent

The potential for reusability and regeneration of the AOR–PVA–CH composite as an effective adsorbent for lead ions was thoroughly examined. After each adsorption cycle, the blend

Table 6 Adsorption isotherm parameters for the adsorption of Pb(II) on AOR–PVA–CH blends

Type of adsorption isotherm	Parameters and values
Freundlich	K_f = 0.1444 $1/n$ =0.9057 R^2 = 0.9882
Langmuir	q_{max} (mg g^{-1}) = 66.66 K_L = 0.002488 R_L = 0.9877 R^2 = 0.9988
Temkin	K_T (L mg^{-1}) = 10.34 B_T (J mol^{-1}) = 0.0810 R^2 = 0.8405

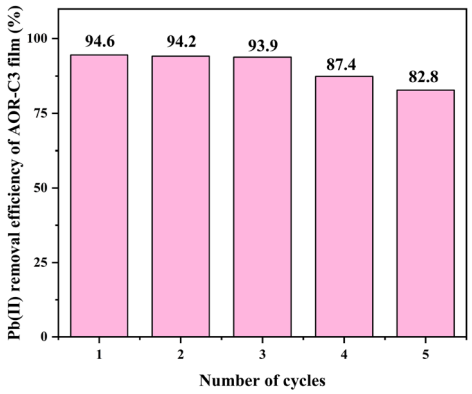

Fig. 14 Reusability of the AOR-C3 film.

was subjected to a desorption process using 0.01 M HCl solution for 5 minutes, followed by thorough washing and drying. The film exhibited efficient regeneration potential, retaining significant adsorption capacity over three cycles, as shown in Fig. 14. This highlights the potential of the AOR–PVA–CH blend as a cost-effective, eco-friendly adsorbent for long-term Pb(II) removal applications.

3.8. Proposed mechanism of lead adsorption

The adsorption of lead ions (Pb^{2+}) onto an organic residue from the arecanut-incorporated PVA–chitosan blend involves a synergistic proposed mechanism (Fig. 15) combining complexation and electrostatic attraction.[75,76] The lead ions in the aqueous solution interact with active functional groups present on the film surface, such as hydroxyl groups from PVA, amino groups from chitosan, and hydroxyl, ester, amine, and carboxyl groups from AOR. These groups form stable chelation complexes with lead ions, enhancing adsorption efficiency. The negatively charged groups present in the film attract the positively charged lead ions *via* electrostatic interactions.

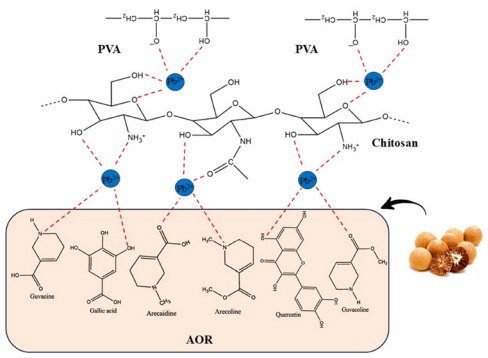

Fig. 15 Proposed mechanism of Pb(II) adsorption by AOR–PVA–CH blends.

4. Conclusions

This research highlights the effective incorporation of waste organic residue from arecanut (AOR) into PVA–CH films, presenting an environmentally sustainable approach for eliminating harmful Pb(II) ions from aqueous solutions. Characterization revealed the semi-crystalline and cross-linked structure of the polymer blend, with enhanced surface properties like the presence of active functional groups, increased roughness and surface area due to AOR incorporation, which significantly improved its adsorption capacity. Changes in the XRD patterns and FTIR spectra recorded before and after adsorption clearly confirm the successful interaction of Pb(II) ions with the adsorbent surface. The results of optimisation studies revealed that the AOR-C3 sample exhibited the highest performance, achieving a removal efficiency of 94.6% for 5 ppm Pb(II) under optimal conditions of 0.5 g adsorbent dosage, 60 minutes contact time, 70 °C, and pH 6. Kinetic analysis aligned with a pseudo-second-order model, and isotherm studies confirmed monolayer adsorption on a homogeneous surface described by the Langmuir model. Reusability tests showed consistent efficiency over three cycles. This study underscores the importance of utilising agricultural residues to develop cost-effective, sustainable, and efficient adsorbents, offering a practical solution to mitigate environmental pollution while valorizing waste materials.

Author contributions

Jasmine Jose: methodology, formal analysis, investigation, data curation, and writing – original draft; Binish CJ: software, methodology, validation, and writing – review and editing; Jobish Johns: conceptualization, resources, and writing – review and editing; Aniz CU: resources and software; Sony J Chundattu: resources, software, and validation; Vijayasankar AV: conceptualization, writing – review and editing, validation, and project administration.

Conflicts of interest

There are no conflicts to declare.

Data availability

Data will be made available on request.

Acknowledgements

The authors gratefully acknowledge the Interdisciplinary Research Centre for Refining and Advanced Chemicals (IRC-RAC), King Fahd University of Petroleum & Minerals, Dhahran, for providing access to various characterization facilities essential for this research.

References

1 S. A. Razzak, M. O. Faruque, Z. Alsheikh, L. Alsheikhmohamad, D. Alkuroud, A. Alfayez, S. M. Z. Hossain and M. M. Hossain, *Environ. Adv.*, 2022, **7**, DOI: 10.1016/j.envadv.2022.100168.
2 P. Saravanan, V. Saravanan, R. Rajeshkannan, G. Arnica, M. Rajasimman, G. Baskar and A. Pugazhendhi, *Environ. Res.*, 2024, **258**, DOI: 10.1016/j.envres.2024.119440.
3 C. Hui, Y. Guo, H. Li, C. Gao and J. Yi, *Sci. Rep.*, 2022, **12**, DOI: 10.1038/s41598-022-11051-9.
4 C. J. Binish, A. V. Vijayasankar and M. P. Sham Aan, *Mater. Today: Proc.*, 2022, **62**, 5182–5188, DOI: 10.1016/j.matpr.2022.02.629.
5 R. Pant, N. Mathpal, R. Chauhan, A. Singh and A. Gupta, in *Mercury Toxicity Mitigation: Sustainable Nexus Approach*, ed. N. Kumar, Springer Nature Switzerland, Cham, 2024, pp. 93–115, DOI: 10.1007/978-3-031-48817-7_4.
6 T. E. Oladimeji, M. Oyedemi, M. E. Emetere, O. Agboola, J. B. Adeoye and O. A. Odunlami, *Heliyon*, 2024, **10**, DOI: 10.1016/j.heliyon.2024.e40370.
7 R. Saini and P. Kumar, in *Heavy Metal Contamination in Wastewater and Its Bioremediation by Microbial-Based Approaches*, ed. V. Singh, V. Mishra, S. N. Rai and M. P. Shah, Springer Nature Singapore, Singapore, 2025, pp. 1–21, DOI: 10.1007/978-981-96-7878-5_1.
8 A. Monroy-Licht, W. J. Martinez-Burgos, J. C. de Carvalho, M. Cavali, A. L. Woiciechowski, S. G. Karp, C. R. Soccol, A. C. De la Parra-Guerra, R. Pozzan and R. Acevedo-Barrios, *Environ. Sci. Pollut. Res.*, 2025, **32**, 20844–20878, DOI: 10.1007/s11356-025-36792-8.
9 P. S. Nishmitha, K. A. Akhilghosh, V. P. Aiswriya, A. Ramesh, M. Muthuchamy and A. Muthukumar, *J. Hazard. Mater. Adv.*, 2025, **18**, DOI: 10.1016/j.hazadv.2025.100755.
10 G. I. Edo, P. O. Samuel, G. O. Oloni, G. O. Ezekiel, V. O. Ikpekoro, P. Obasohan, J. Ongulu, C. F. Otunuya, A. R. Opiti, R. S. Ajakaye, A. E. A. Essaghah and J. J. Agbo, *Chem. Ecol.*, 2024, **40**, 322–349, DOI: 10.1080/02757540.2024.2306839.
11 C. Gundacker, M. Forsthuber, T. Szigeti, R. Kakucs, V. Mustieles, M. F. Fernandez, E. Bengtsen, U. Vogel, K. S. Hougaard and A. T. Saber, *Int. J. Hyg. Environ. Health*, 2021, **238**, DOI: 10.1016/j.ijheh.2021.113855.
12 B. Shilani, R. Mehdipour, B. Mousazadeh, Y. Noruzi, S. Hosseini, H. N. Al-Saedi and S. M. Mohealdeen, *Sci. Rep.*, 2024, **14**(1), DOI: 10.1038/s41598-024-66358-6.
13 Y. Fei and Y. H. Hu, *Chemosphere*, 2023, **335**, DOI: 10.1016/j.chemosphere.2023.139077.
14 J. Wu, T. Wang, J. Wang, Y. Zhang and W.-P. Pan, *Sci. Total Environ*, 2021, **754**, DOI: 10.1016/j.scitotenv.2020.142150.
15 R. Wang, Q. Hu, Q. Wang, Y. Xiang, S. Huang, Y. Liu, S. Li, Q. Chen and Q. Zhou, *Sep. Purif. Technol.*, 2022, **284**, DOI: 10.1016/j.seppur.2021.120280.
16 A. E. Gahrouei, A. Rezapour, M. Pirooz and S. Pourebrahimi, *Desalin. Water Treat.*, 2024, **319**, DOI: 10.1016/j.dwt.2024.100446.
17 Y. Mei, S. Zhuang and J. Wang, *Sci. Total Environ.*, 2025, **968**, DOI: 10.1016/j.scitotenv.2025.178898.
18 Md. G. Azam, M. H. Kabir, Md. A. A. Shaikh, S. Ahmed, M. Mahmud and S. Yasmin, *J. Water Process Eng.*, 2022, **46**, DOI: 10.1016/j.jwpe.2022.102597.
19 I. R. Chowdhury, S. Chowdhury, M. A. J. Mazumder and A. Al-Ahmed, *Appl. Water Sci.*, 2022, **12**, DOI: 10.1007/s13201-022-01703-6.
20 A. Akinterinwa, U. Reuben, J. U. Atiku and M. Adamu, *Carbohydr. Polym.*, 2022, **290**, DOI: 10.1016/j.carbpol.2022.119463.
21 U. Upadhyay, I. Sreedhar, S. A. Singh, C. M. Patel and K. L. Anitha, *Carbohydr. Polym.*, 2021, **251**, DOI: 10.1016/j.carbpol.2020.117000.
22 K. Ahmad, H.-R. Shah, M. S. Khan, A. Iqbal, E. Potrich, L. S. Amaral, S. Rasheed, H. Nawaz, A. Ayub, K. Naseem, A. Muhammad, M. R. Yaqoob and M. Ashfaq, *J. Cleaner Prod.*, 2022, **368**, DOI: 10.1016/j.jclepro.2022.133010.
23 H. Kaur, N. Devi, S. S. Siwal, W. F. Alsanie, M. K. Thakur and V. K. Thakur, *ACS Omega*, 2023, **8**, 9004–9030, DOI: 10.1021/acsomega.2c07719.
24 A. Shahzad, B. Aslibeiki, S. Slimani, S. Ghosh, M. Vocciante, M. Grotti, A. Comite, D. Peddis and T. Sarkar, *Sci. Rep.*, 2024, **14**, DOI: 10.1038/s41598-024-68491-8.
25 C. Duan, T. Ma, J. Wang and Y. Zhou, *J. Water Process Eng.*, 2020, **37**, DOI: 10.1016/j.jwpe.2020.101339.
26 Z. Jiao, C. Gao, J. Li, J. Lu, J. Wang, L. Li and X. Chen, *Molecules*, 2024, **29**(3), DOI: 10.3390/molecules29030660.
27 M. H. Dehghani, S. Afsari Sardari, M. Afsharnia, M. Qasemi and M. Shams, *Sci. Rep.*, 2023, **13**, DOI: 10.1038/s41598-023-29674-x.
28 K. S. Sopanrao and I. Sreedhar, *Sep. Purif. Technol.*, 2024, **340**, DOI: 10.1016/j.seppur.2024.126731.
29 M. A. A. Aljar, S. Rashdan, A. Almutawah and A. A. El-Fattah, *Gels*, 2023, **9**(4), DOI: 10.3390/gels9040328.
30 S. Sharma, P. Sharma, K. Johnson, Y. Madan, S. Li, G. Cai, I. Brahmbhatt, W. Borges and B. Hsiao, *Sep. Sci. Technol.*, 2022, **15**, 87–95, DOI: 10.1016/B978-0-323-90763-7.00004-4.
31 N. S. Mohd Makhtar, J. Idris, M. Musa, Y. Andou, K. H. Ku Hamid and S. W. Puasa, *Processes*, 2021, **9**(1), DOI: 10.3390/pr9010037.
32 Q. Wang, S. Zhu, C. Xi and F. Zhang, *Front. Chem.*, 2022, **10**, DOI: 10.3389/fchem.2022.814643.
33 N. A. A. Qasem, R. H. Mohammed and D. U. Lawal, *npj Clean Water*, 2021, **4**(36), DOI: 10.1038/s41545-021-00127-0.
34 S. Jadoun, J. P. Fuentes, B. F. Urbano and J. Yáñez, *J. Environ. Chem. Eng.*, 2023, **11**, DOI: 10.1016/j.jece.2022.109226.

35 J. Ghaderi, S. F. Hosseini, N. Keyvani and M. C. Gómez-Guillén, *Food Hydrocolloids*, 2019, **95**, 122–132, DOI: 10.1016/j.foodhyd.2019.04.021.
36 B. Samiey, C.-H. Cheng and J. Wu, *Materials*, 2014, **7**(2), 673–726, DOI: 10.3390/ma7020673.
37 N. E. H. Brirmi, T. Chabbah, S. Chatti, K. Alimi, H. Ben Romdhame, R. Mercier, C. Marestin and N. Jaffrezic-Renault, *Water Emerging Contam. Nanoplast.*, 2024, **3**(4), DOI: 10.20517/wecn.2024.60.
38 O. Afolabi, P. Musonge and F. Babatunde, *J. Environ. Health Sci. Eng.*, 2021, **19**(3), DOI: 10.1007/s40201-021-00632-x.
39 P. S. Bharti and N. Kumar, *Appl. Water Sci.*, 2018, **8**, DOI: 10.1007/s13201-018-0765-z.
40 C. Nnaji, C. Ebeagwu and E. Ugwu, *BioResources*, 2017, **12**(1), 799–818, DOI: 10.15376/biores.12.1.799-818.
41 L. Nemeş and L. Bulgariu, *Open Chem.*, 2016, **14**(1), DOI: 10.1515/chem-2016-0019.
42 O. Afolabi, P. Musonge and B. Bakare, *Sci. Afr.*, 2021, **13**(12), DOI: 10.1016/j.sciaf.2021.e00931.
43 R. Pandey, N. Ansari, R. Prasad and R. Murthy, *Am. J. Environ. Prot.*, 2014, **2**(3), 51–58, DOI: 10.12691/env-2-3-1.
44 A. Elkhaleefa, I. Ali, E. Brima, I. Shigidi, A. Elhag and B. Abdalla, *Processes*, 2021, **9**(3), DOI: 10.3390/pr9030559.
45 S. Mallakpour and F. Motirasoul, *J. Cleaner Prod.*, 2019, **224**, 592–602, DOI: 10.1016/j.jclepro.2019.03.229.
46 T. Abraham, R. Kumar, R. Misra and S. K. Jain, *J. Appl. Polym. Sci.*, 2012, **125**(S1), E670–E674, DOI: 10.1002/app.35666.
47 N. A. Ekrayem, A. A. Alhwaige, W. Elhrari and M. Amer, *J. Environ. Chem. Eng.*, 2021, **9**(6), DOI: 10.1016/j.jece.2021.106628.
48 B. C. John, V. Viswambaram, S. Raj and S. Mankunipoyil, *Mater. Today Commun.*, 2023, **34**, DOI: 10.1016/j.mtcomm.2023.105315.
49 J. Jose, C. J. Binish, J. Johns, S. J. Chundattu and A. V. Vijayasankar, *Curr. Appl. Phys.*, 2025, **80**, 43–50, DOI: 10.1016/j.cap.2025.08.012.
50 Y. Jampafuang, A. Tongta and Y. Waiprib, *Polymers*, 2019, **11**(12), DOI: 10.3390/polym11122010.
51 C. J. Binish, I. Kopparappu, A. V. Vijayasankar, A. M. John and S. J. Chundattu, *J. Appl. Polym. Sci.*, 2023, **140**(46), DOI: 10.1002/app.54778.
52 D. Wang, D. Zhang, P. Li, Z. Yang, Q. Mi and L. Yu, *Nano-Micro Lett.*, 2021, **13**(1), DOI: 10.1007/s40820-020-00580-5.
53 D. More, M. Moloto, N. Moloto and K. Matabola, *Int J. Polym. Sci.*, 2021, **2021**, 1–12, DOI: 10.1155/2021/6217609.
54 F. Liao, K. Fu, W. Zhang, H. Song, Y. Kong, Z. Wang and J. Tang, *Sci. Rep.*, 2025, **15**, DOI: 10.1038/s41598-025-96970-z.
55 J. R. Hanumantu, *Nat., Environ. Pollut. Technol.*, 2021, **20**(2), DOI: 10.46488/NEPT.2021.v20i02.012.
56 G. Acik, M. Kamaci, B. Özata and C. Cansoy, *Turk. J. Chem.*, 2019, **43**(1), 137–149, DOI: 10.3906/kim-1801-68.
57 M. B. Mohamed and M. H. Abdel-Kader, *Mater. Chem. Phys.*, 2020, **241**, DOI: 10.1016/j.matchemphys.2019.122285.
58 M. Abureesh, A. Oladipo and M. Gazi, *Int. J. Biol. Macromol*, 2016, **90**, 75–80, DOI: 10.1016/j.ijbiomac.2015.10.001.
59 G. Kovtun, D. Casas and T. Cuberes, *Polymers*, 2024, **16**(17), DOI: 10.3390/polym16172421.
60 J. Jose, B. CJ, J. Johns, H. G, M. MV, S. J. Chundattu and V. A. V, *J. Polym. Res.*, 2025, **33**, DOI: 10.1007/s10965-025-04705-5.
61 C. Branca, G. D'Angelo, C. Crupi, K. Khouzami, S. Rifici, G. Ruello and U. Wanderlingh, *Polymer*, 2016, **99**, 614–622, DOI: 10.1016/j.polymer.2016.07.086.
62 A. Laaraibi, F. Moughaoui, F. Damiri, A. Ouaket, I. Charhouf, S. Hamdouch, A. Jaafari, A. Abdelmjid, N. Knouzi, A. Bennamara and M. Berrada, Chitosan-Clay Based (CS-NaBNT) Biodegradable Nanocomposite Films for Potential Utility in Food and Environment, *Chitin-Chitosan - Myriad Functionalities in Science and Technology*, Intech-Open, 2018, DOI: 10.5772/intechopen.76498.
63 J. Jose, C. J. Binish, J. Johns, S. J. Chundattu and A. V. Vijayasankar, *Ind. Crops Prod.*, 2024, **222**, DOI: 10.1016/j.indcrop.2024.120013.
64 A. Soliman, H. Mohamed Elwy, T. Thiemann, Y. Majedi, F. G. Labata and N. Al-Rawashdeh, *J. Taiwan Inst. Chem. Eng.*, 2016, **58**, 264–273, DOI: 10.1016/j.jtice.2015.05.035.
65 X. Chen, X. Jin, C. Zhang, Z. Jiao, Z. Yang, K. Wang, J. Li and Q. Zhang, *Molecules*, 2024, **29**(23), DOI: 10.3390/molecules29235589.
66 B. C. J, A. John, S. Chundattu, S. Mankunipoyil and V. Viswambaram, *J. Polym. Res.*, 2023, **30**(12), DOI: 10.1007/s10965-023-03833-0.
67 A. Mihaela Predescu, E. Matei, M. Râpă, C. Pantilimon, G. Coman, S. Savin, E. Elisabeta Popa and C. Predescu, *Anal. Lett.*, 2019, **52**, 2365–2392, DOI: 10.1080/00032719.2019.1588286.
68 V. Singh, N. Singh, S. N. Rai, V. K. Chaturvedi, S. K. Singh, A. Kumar, E. Vamanu and V. Mishra, *Nanocomposites*, 2024, **10**, 201–213, DOI: 10.1080/20550324.2024.2347804.
69 M. Wahyuhadi, R. Kusumadewi and R. Hadisoebroto, *IOP Conf. Ser. Earth Environ. Sci.*, 2023, **1203**, DOI: 10.1088/1755-1315/1203/1/012035.
70 W.-J. He, Y.-F. He, D.-Z. Yan, Y. Wang and R.-M. Wang, *J. Dispers Sci. Technol.*, 2014, **35**, 1378–1385, DOI: 10.1080/01932691.2013.845104.
71 M. R. Karim, M. O. Aijaz, N. H. Alharth, H. F. Alharbi, F. S. Al-Mubaddel and Md. R. Awual, *Ecotoxicol. Environ. Saf.*, 2019, **169**, 479–486, DOI: 10.1016/j.ecoenv.2018.11.049.
72 J. Ayach, L. Duma, A. Badran, A. Hijazi, A. Martinez, M. Bechelany, E. Baydoun and H. Hamad, *Materials*, 2024, **17**(11), DOI: 10.3390/ma17112724.
73 C. Ji, D. Wu, J. Lu, C. Shan, Y. Ren, T. Li, L. Lv, B. Pan and W. Zhang, *Water Res.*, 2021, **189**, DOI: 10.1016/j.watres.2020.116599.
74 A. Ebelegi, N. Ayawei and W. Donbebe, *Open J. Phys. Chem.*, 2020, **10**, 166–182, DOI: 10.4236/ojpc.2020.103010.
75 Sh. M. Khaliullin, V. D. Zhuravlev, V. G. Bamburov, A. A. Khort, S. I. Roslyakov, G. V. Trusov and D. O. Moskovskikh, *J. Solgel Sci. Technol.*, 2020, **93**, 251–261, DOI: 10.1007/s10971-019-05189-8.
76 N. Bombuwala Dewage, R. E. Fowler, C. U. Pittman, D. Mohan and T. Mlsna, *RSC Adv.*, 2018, **8**(45), 25368–25377, DOI: 10.1039/C8RA04600J.